PAPER

Check for updates

Spectral diversities of chromophoric dissolved organic matter in paddy field water adjacent to black soil regions of Northeast China

Zhong Lv, [ID] [a] Chunyu Liu,[ab] Jianbo Wang,[ac] Changming Li,[a] Xing Teng[d] and Yong Tan*[a]

Dissolved organic matter (DOM) plays a crucial role in the aquatic ecosystem of rice paddies, and its content reveals the transport relationship of soil nutrients absorbed by rice seedlings, but there are few reports on this in the black soil. This paper analyzed the concentration of chromophoric dissolved organic matter (CDOM) in irrigation water of black soil in Wanchang Town, Jilin Province, China, using combination detection technology of excitation–emission matrix (EEM) spectroscopy and UV-vis absorption spectroscopy and correlational analysis. Four results demonstrated the CDOM characteristics of the black soil. The UV-vis absorption coefficient $a375$ is correlated positively with CDOM concentration and molecular weight, indicating the presence of macromolecular organics. E_4/E_6 is negatively correlated with the spectral slope S_R, with DOM dominated by humic acid and protein-like substances. The peak of the EEM spectrum has an average frequency shift difference of about 20 nm compared to non black soil areas. CDOM content is higher in rice paddy water than in irrigation channels and natural paddy water, influenced by microbial degradation, soil processes, and human inputs. These research results are conducive to optimizing irrigation management, improving water quality and enhancing the level of rice cultivation in the black soil. This combined detection and correlational analysis method effectively identified CDOM sources, offering valuable insights into DOM dynamics in agricultural irrigation systems.

1. Introduction

Dissolved organic matter (DOM) is a complex organic mixture widely present in surface environments such as water, soil, and sediments. Its main components include humic acid, amino acids, polysaccharides, and others.[1–3] DOM plays a critical role in regulating the physical, chemical, and biological properties of aquatic ecosystems, influencing water pH, alkalinity, and charge balance, and is closely linked to the migration and transformation of various elements in the water.[4] As a key component of the global carbon cycle, DOM is significantly affected by climate change and plays a crucial role in the material and energy cycling within ecosystems.[5] The primary sources of DOM are divided into terrestrial and internal sources. Terrestrial sources mainly include atmospheric deposition, effluent from wastewater treatment plants, tributary inflows, and domestic sewage discharge.

The internal sources mainly include organic matter produced by microbial metabolism and death, as well as the degradation of aquatic plants such as algae.[6] Chromophoric dissolved organic matter (CDOM), an important component of DOM, has a highly complex chemical composition and structure. CDOM can influence the migration and transformation of heavy metals or organic pollutants through adsorption, and it also plays a role in the cycling of inorganic nutrients like nitrogen and phosphorus.[7,8] Additionally, CDOM possesses unique optical characteristics. When it was irradiated with UV-visible light, it can undergoes photochemical degradation. Therefore, the use of UV-vis absorption spectroscopy and EEM spectroscopy to study the structure, origin and composition of CDOM has become a research hotspot. These techniques are widely used due to their high sensitivity, ease of operation, and minimal sample requirements.[9–11]

Li *et al.* used three-dimensional excitation–emission matrix fluorescence spectroscopy (3D EEM) to characterize DOM, achieving an analysis of the degradability of individual DOM components through regional division of the 3D EEM.[10] Pearson *et al.* used a three-dimensional fluorescence emission matrix to measure the DOM in water bodies in alpine wetlands, and the results showed that the decomposition of organic matter had significant effects on the chemical properties, sources, humification degree and composition of the DOM in water bodies.[12]

[a]Key Laboratory of Spectral Detection Science and Technology, School of Physics, Changchun University of Science and Technology, Changchun, 130032, China

[b]Jilin Zhengyuan Environmental Protection Technology Co., Ltd., Changchun, 130041, China

[c]Jilin Zhengzhen Testing Co., Ltd., Changchun, 130041, China

[d]Jilin Academy of Agricultural Sciences (Northeast Agricultural Research Center of China), Changchun, 130000, China

Liu *et al.* applied EEM spectroscopy combined with UV spectroscopy and parallel factor analysis to study the DOM composition in the Bohai Sea, identifying four types of fluorescence peaks: high-excitation tryptophan (peak S), low-excitation tryptophan (peak T), humic acid-like (peak A), and fulvic acid-like (peak C).[13] They also noted that during the wet season, the influence of external river input on DOM was significant. Zhang *et al.* focused on the surface water of the Beiyun River, using EEM spectroscopy to analyze its DOM, which consisted of tryptophan-like substances, humic acid, and ultraviolet humic acid, revealing the combined effects of terrestrial humic acid substances and biological sources.[14] Yuan *et al.* investigated the impact of water nutrient levels on DOM and found that during the eutrophic summer, UV absorption values were significantly higher than those in the oligotrophic winter, indicating marked differences in water quality under different nutrient conditions.[15] Gao *et al.* demonstrated that the spectral characteristics of DOM in different agricultural soils varied, and the intensity and correlations of its fluorescence components provided a feasible method for characterizing DOM in agricultural soils.[16] The 3D fluorescence method is also crucial for identifying rice quality and evaluating the environmental conditions of rice growth. For example, Suman *et al.* used EEM spectroscopy combined with principal component analysis to identify rice quality under different spatiotemporal conditions.[17] Zhang *et al.* utilized 3D fluorescence technology and the coupling factor method to study the extent of soil erosion in different soil types after rice planting in Northeast China.[18]

This study selected a typical black soil agricultural irrigation watershed in the upper reaches of the Songhua River-Wanchang Town, a major paddy rice-producing area in Jilin Province-as the research area. EEM spectroscopy and UV-vis absorption spectroscopy combined detection method was employed to analyze and characterize the CDOM concentrations in various water bodies within the region. This study aimed to reveal the main composition types and property differences of CDOM, explore the relationships between its composition, concentration, and characteristic parameters, and conduct an in-depth analysis of its sources. The findings provide valuable insights for the healthy growth of rice and the protection of water resource (Table 1).

2. Materials and methods

2.1 Study area overview

Fig. 1(a) and (b) show Wanchang Town, located in Jilin City, Jilin Province (43°45′N, 125°54′E). Situated in the Songhua River Basin within the Songliao Plain-an important black soil main
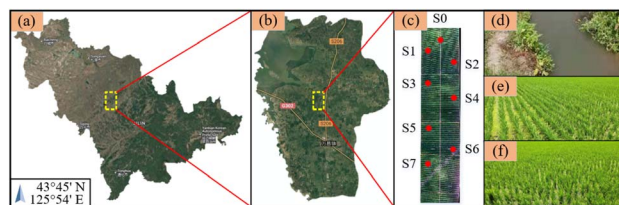

Fig. 1 Satellite image of Jilin Province, Jilin Province is located in the center of Northeast China and the geographical center of Northeast Asia, showing obvious characteristics of high in southeast and low in northwest. (b) Wanchang Town of Jilin Province is located in the valley plain area on the east bank of Yinma River, which is located in the fine japonica rice planting belt at 43° north latitude. (c) The water samples sampled in this study (S0–S7) were photographed by UAV. (d) Ditch water (S0) for the irrigation of experimental and natural fields. (e) The sampling experiment field (S1–S5) was planted by artificial rice transplanting. (f) Sampled natural fields for planting using artificial transplanting (S6 and S7).

grain producing area, it lies in the northern temperate zone of the Northern Hemisphere. The region enjoys a temperate continental monsoon climate, with an average altitude of 210 m, an annual average temperature of 5.2 °C, and an average annual precipitation of 612.2 mm. The average annual sunshine duration is 2596.8 h, with the crop growing season spanning from April to September, during which sunshine lasts 1500–1600 h, and the frost-free period ranges from 138 to 145 days.[19] Favorable rainfall and heat from July to August support rice growth, while the diurnal temperature difference of 11.4 °C during the heading to maturity stage (August to September) promotes nutrient accumulation in rice. The soil is paddy soil with a loam texture, organic matter content greater than or equal to 2%, average total nitrogen content of 0.15%, and a pH range of 5.5–6.5.[20,21]

Wanchang Town lies in the center of the world's golden rice belt and is a key rice production zone in Northeast China. In 2018, it was recognized as a model town for agricultural industrialization by China and designated a "Green Industry Demonstration Park" by the United Nations Industrial Development Organization, highlighting its representativeness for this study.

2.2 Sample collection and processing

Considering the spatial distribution characteristics of planting sampling points, water quality sampling points are shown in Fig. 1(c). Three types of water samples were collected in this study, as shown in Fig. 1(d)–(f). A total of 8 water samples were collected, labeled as S0 to S7. Among these, samples S0 was

Table 1 Method advantage comparison table

Parameter	This study	Traditional methods	Advantages
Detection technique	UV-vis + EEM + correlation analysis	Single spectroscopy	Multi-dimensional, high sensitivity
Differentiation	20 nm peak shift marker	Chemical extraction	Non-destructive, rapid
Field applicability	Real-time monitoring	Lab analysis	Field decision support
Cost & complexity	Moderate (spectrometer)	High (*e.g.*, HPLC-MS)	Agricultural feasibility

from the irrigation canal, samples S1 to S5 were from the experimental field, and S6 to S7 were from the natural paddy field. Brown polyethylene plastic bottles were used to collect the water samples, which were then immediately stored in a 4 °C constant temperature refrigerator and transported back to the laboratory for preservation. Before analysis, the water samples were equilibrated to room temperature (25 °C) and filtered through a 0.45 μm membrane filter. The subsequent water quality routine indicators and spectral measurements were completed within 12 h after sampling. The selected experimental plots included irrigation canal water (S0, flowing from north to south) and experimental and natural fields distributed on either side. Among them, S1–S5 represent paddy field water samples from five different rice varieties, while S6 and S7 are paddy field water samples from the same rice variety in natural fields. In the study, it is assumed that the irrigation water quality and soil quality of the experimental and natural fields are consistent.

2.3 Absorption spectrum characterization analysis

The UV-visible absorption spectra of the water samples were measured using a UV-1900 spectrophotometer (Shimadzu Instruments, Suzhou, China), with a scanning range of 200–800 nm, a spectral bandwidth of 1.0 nm, and a 10 mm pathlength quartz cuvette. The instrument is equipped with a LO-RAY-LIGH low stray light diffraction grating, which effectively minimizes stray light interference and enables baseline scattering correction. Furthermore, to eliminate Rayleigh and Raman scattering effects, first- and second-order scattering regions were automatically identified and excluded using built-in software during subsequent EEM data processing, ensuring the reliability of the spectral analysis.

Fluorescence excitation–emission matrix (EEM) spectra were acquired using an LS-55 fluorescence spectrometer (Perkin-Elmer, USA), with ultrapure water serving as the blank. The excitation source was a 20 kW pulsed xenon lamp with ozone-free emission. Excitation wavelengths (Ex) were scanned from 208 to 403 nm, and emission wavelengths (Em) from 198 to 798.5 nm, both at 5 nm increments. The scanning speed was set to 1500 nm min^{-1}. Compared with conventional two-dimensional fluorescence spectra, three-dimensional EEM spectra capture comprehensive fluorescence characteristics under multiple excitation–emission wavelength combinations. This allows for more accurate differentiation between humic-like and protein-like components in DOM, reduces the risk of misinterpretation due to spectral overlap, and is especially suited for identifying the sources and components of CDOM in complex aquatic environments.

To minimize the influence of dissolved inorganic carbon (DIC) and other inorganic ions on fluorescence signals, all samples were pre-filtered through 0.45 μm membrane filters and acidified with 10% HCl to adjust the pH to approximately 2. The acidified samples were then degassed for 30 minutes to remove carbonate species. Additionally, inner filter effects (IFE) were corrected by measuring the absorbance of each sample at the corresponding excitation and emission wavelengths prior to

EEM acquisition, ensuring that total absorbance remained below 0.3 to avoid fluorescence quenching and signal distortion.

2.4 Data analysis methods

In this study, UV-vis absorption spectrum and EEM spectrum were used to analyze water samples. The relevant spectral parameters are shown in Table 2.

2.5 Data correlation analysis method

In this study, the Pearson correlation analysis method was employed to analyze the correlation between the aforementioned water quality parameters. Pearson correlation analysis is a classical statistical method used to quantitatively study the linear relationship between variables. In this research, it was applied to explore the correlations among water sample indicators and their statistical significance. By calculating the correlation coefficient (r) and the significance level (P-value), the potential dependencies between various water quality parameters can be revealed, providing a scientific basis for understanding the dynamic changes in water quality.

The Pearson correlation coefficient (r) ranges between [−1,1]. When $r > 0$, it indicates a positive correlation; when $r < 0$, it indicates a negative correlation; and when $r = 0$ it suggests no correlation. The closer the absolute value of r is to 1, the stronger the correlation. The formula for calculating r is as follows:

$$r = \frac{\sum \left(X_i - \overline{X} \right) \left(Y_i - \overline{Y} \right)}{\sqrt{\sum \left(X_i - \overline{X} \right)^2 \left(Y_i - \overline{Y} \right)^2}} \tag{1}$$

here X_i and Y_i represent the sample data, and $\overline{X}$ and $\overline{Y}$ are the mean values of variables X and Y, respectively.

The statistical significance (P-value) is used to test whether the correlation coefficient is significant. When $P < 0.05$, the correlation is considered significant, while $P \geq 0.05$ indicates that the correlation is not significant.

To further enhance the analysis of data correlations, this study also employed the confidence limit (CL), also referred to as the confidence interval (CI). CI is used to estimate the possible range of the correlation coefficient and reflects the reliability of the results.

3. Results analysis of routine indexes of water quality

In this study, the total phosphorus (TP) was determined using the method described in the "water quality-determination of orthophosphate and total phosphorus-continuous flow analysis(CFA) and ammonium molybdate spectro-photometry",[31] total nitrogen (TN) was measured using the "water quality-determination of total nitrogen-alkaline potassium persulfate digestion UV spectrophotometric method",[32] ammonia nitrogen (NH$_3$–N) was analyzed using the "water quality-determination of ammonia nitrogen-Nessler's reagent spectro-photometry",[33] and total organic carbon (TOC) was determined

Table 2 Vibrational band attribution in rice spectrum

Argument	Calculation formula	Formula parameters and description
Absorption coefficient (a)	$\alpha_{(\lambda)} = 2.303 D_{(\lambda)}/l$	$D_{(\lambda)}$ represents the absorbance at wavelength λ, and l is the path length of the light (in meters)[22]
Spectral slope (S_R)	$S_R = S_{(275-295)}/S_{(350-400)}$ $\alpha_{(\lambda)} = \alpha_{(\lambda_0)}\exp[S_{(\lambda_0 - \lambda)}]$	S represents the spectral slope, λ_0 is the reference wavelength (in nm). $S_{(275-295)}$ and $S_{(350-400)}$ correspond to the wavelength ranges from 270 nm to 350 nm and from 350 nm to 400 nm, respectively. The S value is related to the structure and relative molecular weight of chromophoric dissolved organic matter (CDOM). A higher S value indicates that the CDOM has a smaller relative molecular weight, suggesting the presence of smaller, simpler organic molecules, while a lower S value implies larger, more complex molecules[23]
Ratio method (E_4/E_6)	$E_4/E_6 = \alpha_{(465)}/\alpha_{(665)}$	This ratio is used to characterize the changes in the degree of aromatization and relative molecular weight of CDOM solution during photodegradation. The lower the value, the larger the relative molecular weight of the solution and the higher the degree of aromatization[24]
Fluorescence index (FI)	$FI = I_{Em = 470\ nm}/I_{Em = 520\ nm}$	The fluorescence index (FI) is calculated as the fluorescence intensity ratio between emission wavelengths of 470 nm and 520 nm when the excitation wavelength (Ex) is set to 370 nm. It is used to characterize the source of chromophoric dissolved organic matter (CDOM). FI > 1.9 indicates that the CDOM is primarily of autochthonous origin, mainly derived from microbial activity. FI < 1.4 suggests that the CDOM is predominantly from terrestrial sources, with a lower contribution from microbial activity[25,26]
Autogenetic index (BIX)	$BIX = I_{E_m = 380\ nm}/I_{E_m = 430\ nm}$	The BIX (biological index) is calculated as the fluorescence intensity ratio between emission wavelengths of 380 nm and 430 nm when the excitation wavelength (Ex) is set to 310 nm. It is used to characterize the relative contribution of autochthonous sources in CDOM. The BIX value increases with the prominence of autochthonous characteristics. The higher the BIX value, the higher the bioavailability of CDOM. In other words, the larger the BIX value, the more significant the contribution from biological sources and the higher the potential for biological utilization[27,28]
Humification index (HIX)	$HIX = \dfrac{\int I_{E_m = 435-480\ nm}}{\int I_{E_m = 300-345\ nm}}$	The humification index (HIX) is calculated as the ratio of the integrated fluorescence intensity in the 435 nm to 480 nm emission range to that in the 300–345 nm emission range, using an excitation wavelength of 254 nm. This index is used to characterize the humification degree of chromophoric dissolved organic matter (CDOM). A higher HIX value indicates a higher degree of humification, meaning that the CDOM has a more complex structure and is more decomposed. Conversely, a lower HIX value suggests a fresher, less decomposed form of organic matter. The HIX provides insights into the complexity of CDOM's structure and its origin, with higher values often associated with terrestrial inputs and microbial degradation processes[29,30]

using the "water quality-determination of total organic carbon-combustion oxidation nondispersive infrared absorption method".[34] Table 3 presents the routine water quality parameters obtained from the water samples collected in the study area.

From the data in Table 3, the irrigation water from the ditch (S0) is sourced from underground extracted well water, and according to the "ground water quality standards",[35] it falls under category IV water, suitable for agricultural use. It can also be analyzed that there is a significant difference in water quality between the experimental field samples (S1–S5) and the natural field samples (S6–S7). The experimental field water samples show relatively stable and lower levels of indicators such as total phosphorus (TP), total nitrogen (TN), ammonia nitrogen (NH$_3$–N), and total organic carbon (TOC), indicating better control over fertilizer application amounts and uniformity in the experimental fields.

3.1 Absorption spectrum characterization analysis

From Fig. 2, it can be observed that the absorbance of the water samples S0 to S7 remains nearly unchanged in the range from 400 nm to 800 nm, with the spectral curves overlapping

Table 3 Water quality routine index table of S0–S7 water sample

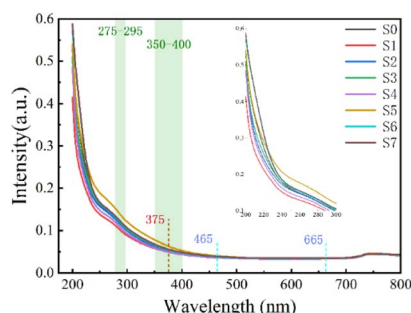| Paddy field number	(TP) (mg L^{-1})	(TN) (mg L^{-1})	(NH$_3$–N) (mg L^{-1})	(TOC) (mg L^{-1})
S0	0.010	0.864	0.750	1.49
S1	2.105	9.763	13.329	19.12
S2	2.197	11.621	15.117	20.03
S3	2.388	10.411	14.137	19.83
S4	2.023	11.146	13.848	20.16
S5	2.081	10.800	13.617	19.16
S6	2.938	12.139	21.003	26.33
S7	2.481	11.794	20.253	25.47

Fig. 2 UV-vis absorption spectra of water samples S0–S7. The red lines indicate the absorption coefficient (a) values, the blue lines represent the spectral range for the ratio method (E_4/E_6), and the green lines highlight the spectral slope (S_R) values.

significantly. This suggests that the optical properties of these samples in the visible light range are similar, likely due to comparable concentrations or compositions of dissolved organic matter (CDOM). However, in the ultraviolet (UV) range (200 nm to 400 nm), the absorbance of the water samples S0 to S7 shows significant variation, with noticeable differences. For example, S0 almost overlaps with S2 and S5 after 263 nm and before 213 nm, respectively. At 375 nm, the absorption intensity is ranked from high to low as S5, S7, S6, S3, S0 and S2, S1 and S4. S6 and S7 basically coincide because both are sampled natural fields for planting using artificial transplanting. This indicates that the UV region is a sensitive zone for characterizing the CDOM composition and water quality characteristics of these samples. In the UV range, changes in absorbance are typically related to the aromaticity or concentration of CDOM. Higher absorbance may indicate the presence of more aromatic compounds or other substances with stronger light absorption properties.

Table 4 Analysis parameter table of S0–S7 water sample

Paddy field number	a(375)	E_4/E_6	S_R
S0	11.976	1.088	0.720
S1	11.515	1.055	0.808
S2	11.976	1.059	0.686
S3	12.436	1.088	0.639
S4	11.285	1.059	0.751
S5	14.509	1.143	0.569
S6	12.667	1.086	0.666
S7	12.897	1.114	0.637

By extracting the three types of water samples (S0–S7) from the spectral data in Fig. 2 and applying the calculation methods outlined in Table 3, the corresponding parameters for each water sample, as displayed in Table 4, were obtained.

The study employed Pearson correlation analysis to explore the linear relationships among CDOM parameters a(375), E_4/E_6, and S_R. Data were tested to ensure compliance with normality and linearity assumptions. The results, shown in Table 5, indicate significance at the $P < 0.01$ level. After multiple comparisons with Bonferroni correction, a significant negative correlation between a(375) and E_4/E_6 (−0.8537, 95% CI: −0.90 to −0.80) remained, indicating that higher a(375) values correspond to DOM with larger molecular weight and greater aromaticity. Similarly, a(375) showed a negative correlation with S_R (−0.8953, 95% CI: −0.91 to −0.83), reinforcing the connection between DOM complexity and CDOM concentration. A positive correlation was observed between E_4/E_6 and S_R (0.9397, 95% CI: 0.92 to 0.96), suggesting that DOM with lower molecular weight exhibits higher spectral slope ratios. These findings highlight the molecular composition dynamics of CDOM in agricultural irrigation water, particularly the interactions between humic acid substances and microbial degradation products.

3.2 EEM spectroscopy analysis

3.2.1 Fluorescence peak characteristics. Fluorescence peaks were identified at 8 sampling points of the water samples. As shown in Fig. 3, peaks A and C were humic acid-like peaks, while B and T were protein-like peaks. The former are typically associated with terrestrial soil inputs via runoff or the release of humic acid substances from paddy field sediments,[38] while the latter are primarily generated by the endogenous activities of microorganisms, algae, and plankton.[39,40] All water samples exhibited these four fluorescence peaks except of weak peak T in S0. The results also showed that ranges of four fluorescence peaks are namely humus peak A ($\lambda_{Ex}/\lambda_{Em}$ = 210–260/360–500) in the ultraviolet region, frericic acid peak C ($\lambda_{Ex}/\lambda_{Em}$ = 310–330/360–500) in the visible region, tyrosine peak B ($\lambda_{Ex}/\lambda_{Em}$ = 210/280–320) and tryptophan peak T ($\lambda_{Ex}/\lambda_{Em}$ = 250–270/300–310) at short wave. Compared with literature,[36,37] the regional average difference of these peaks is about 20 nm, which could be a significant difference between black soil and other soil types.

Table 5 Analysis parameter table of S0–S7 water sample[a,b,c]

Relative index	$a(375)$	E_4/E_6	S_R	95% confidence interval (CI)	Statistical significance (P-value)
$a(375)$	1	−0.8537**	−0.8953**	(−0.921, −0.785)	<0.01
E_4/E_6		1	0.9397**	(0.899, 0.970)	<0.01
S_R			1	(−0.935, −0.845)	<0.01

[a] ** indicates a significant correlation at the $P < 0.01$ level (two-tailed). [b] Confidence intervals (CI) were calculated to ensure the robustness of correlation coefficients. [c] Statistical tests corrected for multiple comparisons using the Bonferroni method.

This phenomenon may be related to the reduction of aromatic structures in DOM molecules, the disruption of conjugated systems, and the increase in the proportion of small organic molecules, reflecting the simplification trend of DOM structures. The potential mechanisms causing this change may include: on the one hand, the decomposition effect of microorganisms is strengthened, accelerating the degradation of high-molecular organic substances; on the other hand, the insufficient input of exogenous organic matter limits the supply of complex-structured organic matter.

3.2.2 Comparison of fluorescence characteristic parameters. The analysis of fluorescence spectrum parameters, as shown in Fig. 4, provides further clarification of the CDOM source characteristics in paddy water across the experimental area. The fluorescence index (FI) analysis reveals that FI values for the S1–S5 regions range from 1.9 to 1.99, indicating that CDOM in these areas predominantly originates from microbial activities with significant autochthonous characteristics. These high FI values suggest the presence of low-molecular-weight dissolved organic matter produced by microbial metabolism, such as bacteria and algae, which typically exhibit higher fluorescence intensity. In contrast, the FI values for canal water (S0) and naturally grown paddy water (S6 and S7) range from 1.4 to 1.9, specifically at 1.87 and 1.83, respectively. These lower FI values indicate mixed sources of CDOM in these regions, including both microbial autochthonous inputs and terrestrial contributions. Terrestrial CDOM, commonly derived from soil leaching, plant litter, and surface runoff, is often characterized

by high-molecular-weight humic acid substances with lower fluorescence intensity, which accounts for the decreased FI values.

The biological index (BIX) further corroborates these findings. In the experimental paddy fields (S1–S5), BIX values range from 0.77 to 0.82, with most values approaching 0.8, indicating that CDOM in this region is primarily composed of newly formed autochthonous components (BIX > 0.8). Autochthonous CDOM is typically generated through microbial metabolism, phytoplankton activity, and the growth or decomposition of aquatic plants, signifying active microbial processes and a high capacity for generating endogenous organic matter within the
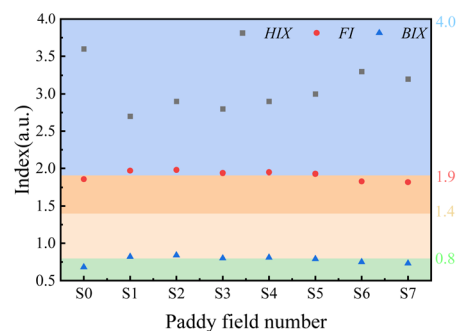

Fig. 4 Fluorescence characteristic parameters of water samples S0–S7. The gray lines indicate the threshold values for the humification index (HIX), the red lines mark the threshold range for the fluorescence index (FI), and the blue lines represent the threshold values for the autogenetic index (BIX).
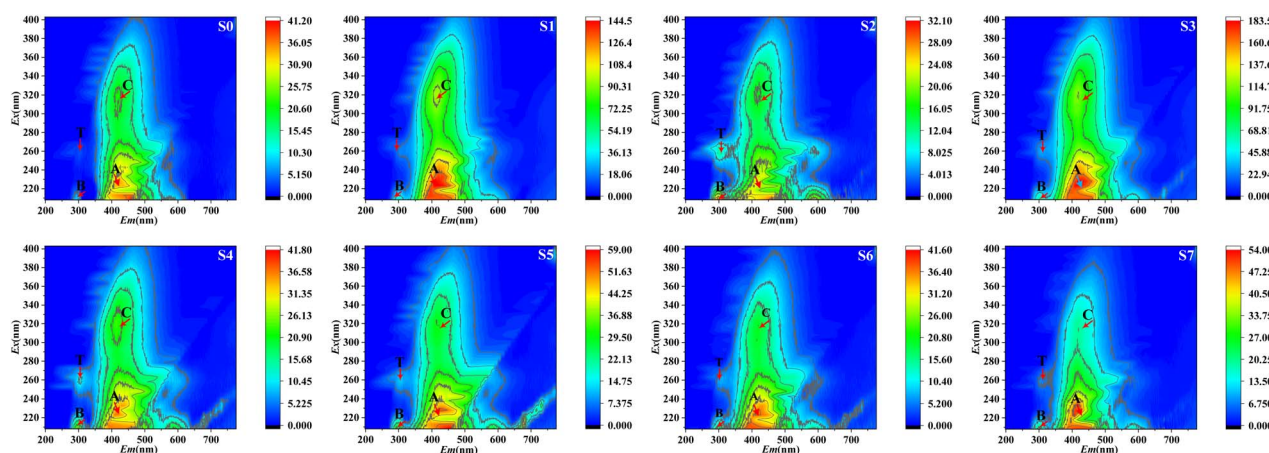

Fig. 3 EEM spectroscopy of DOM in water samples. The locations of peaks A, C, B, and T are marked in the figure.

system. By contrast, the BIX value for canal water (S0) is 0.69, and for naturally grown paddy water (S6–S7), it ranges from 0.71 to 0.74, suggesting a lower contribution of autochthonous CDOM in these waters. Instead, these areas exhibit a stronger influence from terrestrial inputs, which are characterized by high-molecular-weight organic matter that is less bioavailable and slower to degrade.

The BIX values also highlight differences in the degradation potential and self-purification ability of the water bodies. Higher BIX values indicate a greater proportion of autochthonous CDOM, reflecting a stronger capacity for organic matter degradation and endogenous production. This aligns with the FI analysis, where experimental paddy water exhibited higher FI values, confirming substantial microbial contributions, while canal and naturally grown paddy water displayed mixed-source characteristics with more significant terrestrial influences. Together, these findings illustrate the variability in CDOM characteristics and sources across different water bodies, driven by local environmental and microbial processes.

In addition, the humification index (HIX) for all sampling points (S0–S7) is close to 4, indicating that the humification level of CDOM in paddy water is low (HIX < 4). This suggests that the CDOM in the water is mainly composed of relatively fresh, not fully humified substances.

In summary, the CDOM in paddy water in the experimental area is primarily derived from autochthonous microbial activity, exhibiting significant autochthonous characteristics. In contrast, the canal water and natural paddy water exhibit both autochthonous and allochthonous characteristics, with CDOM sourced from both microbial activity within the water body and organic matter from external inputs such as surface runoff. These findings provide important insights for water quality management and ecological environment research.

3.3 Correlation analysis between CDOM fluorescence peak and water quality index

In the analysis of the correlation between CDOM fluorescence peaks and water quality indicators in paddy water, the Pearson correlation coefficient was used. Based on the data in Table 6, the following conclusions can be drawn:

3.3.1 Correlation between peak A and peak C. Both peak A and peak C are humic acid-like substances, and they exhibit a significant correlation. This suggests that the intensities of

these two fluorescence peaks in the water body may be influenced by similar humic sources, and are likely closely related to the humification process of organic matter in the water.

3.3.2 Correlation between peak B and total phosphorus (TP). Peak B shows a high correlation with total phosphorus (TP) in the water. This indicates that the concentration of TP may affect the intensity of peak B, which in turn influences the concentration of tyrosine-like substances. The fluorescence characteristics of tyrosine-like substances mainly originate from phosphorus-containing organic matter in the water, especially organic matter related to phosphate.

3.3.3 Correlation between peak T and total organic carbon (TOC). Peak T shows a high correlation with TOC in the water. This result is consistent with findings from Jiang H and colleagues on domestic wastewater, indicating that the fluorescence intensity of tryptophan-like substances is significantly correlated with TOC concentration.[41] The concentration of tryptophan-like substances is largely dependent on the TOC concentration in the water, particularly in waters with higher organic loads.

4. Discussion

From the fluorescence characteristics of DOM, the concentration of chromatic dissolved organic matter (CDOM) in the experimental paddy field water was relatively high. CDOM concentration showed a significant positive correlation with molecular weight and a negative correlation with spectral slope, indicating the presence of a substantial amount of stable, high-molecular-weight organic matter in the water body.[42] The fluorescence peaks of CDOM included humic acid-like peaks (A and C) and protein-like peaks (B and T), among which the A and C peaks exhibited higher fluorescence intensity in the experimental area, suggesting stronger humic acid characteristics. Compared with irrigation channel water and naturally grown paddy water, the fluorescence intensity in the experimental area was significantly higher. Correlation analysis of fluorescence peaks indicated that these CDOM components shared common sources, highlighting a notable difference between black soil and other soil types.

Fluorescence index (FI) and biological index (BIX) analyses suggested that DOM in the experimental area mainly originated from primary inputs, whereas the DOM in irrigation channels

Table 6 Correlation analysis between fluorescence peak and routine indexes of water samples[a,b]

	Peak A	Peak C	Peak B	Peak T	TP	TN	NH$_3$–N	TOC
Peak A	1	0.972**	0.395	−0.177	0.505	−0.212	−0.009	0.28
Peak C		1	0.345	−0.178	0.339	−0.033	−0.191	0.149
Peak B			1	−0.118	0.731*	−0.58	0.293	0.208
Peak T				1	−0.1096	0.095	0.294	0.659*
TP					1	0.899**	0.631*	0.564
TN						1	−0.84**	−0.445
NH$_3$–N							1	0.525
TOC								1

[a] ** indicates a significant correlation at the $p < 0.01$ level (two-tailed). [b] * indicates a significant correlation at the $p < 0.05$ level (one-tailed).

and naturally grown paddy water exhibited a mix of autochthonous and allochthonous sources. Additionally, the humification index (HIX) revealed that the degree of DOM humification was relatively low across all areas. Finally, correlation analysis between fluorescence peaks and water quality parameters indicated that the concentration of tyrosine-like substances (peak B) was primarily associated with phosphorus-containing.

In addition, the physicochemical properties of black soil play a critical role in the generation and transformation of CDOM. Black soil is characterized by a high organic matter content, particularly rich in humic acid and fulvic acid, both in concentration and proportion, which are key contributors to the increased aromaticity and molecular weight of CDOM. High-molecular-weight and highly aromatic components within humic substances exhibit strong absorption and emission signals in both UV and three-dimensional fluorescence spectra, significantly enhancing the spectral intensity and stability of CDOM. Therefore, the humic acid to fulvic acid ratio in black soil can serve as a key indicator for evaluating the potential of CDOM formation.

This study adopted a natural-state water sample analysis strategy to preserve the authentic CDOM characteristics of paddy waters in black soil regions. Although ambient pH values (measured pH values were highly consistent across all samples, ranging between 6.3 and 6.7) may potentially influence fluorescence signals,[43,44] existing research demonstrates that humic-like substances maintain excellent fluorescence stability within neutral pH ranges (5.5–7.5).[45] We particularly observed that the distinctive 20 nm fluorescence peak shift in black soil regions showed remarkable consistency across all samples, confirming the field applicability of the spectral markers established in this study. Future work could further validate the influence weights of different environmental parameters through controlled experiments, including designed pH gradient tests and long-term monitoring.

5. Conclusion

This study integrated excitation–emission matrix (EEM) fluorescence spectroscopy, ultraviolet-visible (UV-vis) absorption spectroscopy, and biochemical analyses to investigate the characteristics, sources, and agricultural implications of chromophoric dissolved organic matter (CDOM) in irrigation water from black soil paddy fields in Wanchang Town, Jilin Province. The results revealed that CDOM concentrations in experimental paddy water were significantly higher than in irrigation canal water and slightly lower than in natural paddy fields, influenced by microbial degradation, soil leaching, and human activities. A strong negative correlation was observed between $a(375)$ and spectral slope (S_R) ($r = -0.8953$, $p < 0.01$), indicating the presence of stable, high-molecular-weight and highly aromatic organic matter.

Fluorescence peak analysis identified humic-like components (peaks A and C) and protein-like substances (peaks B and T), with the experimental paddies showing dominant autochthonous microbial contributions, in contrast to the mixed sources observed in natural paddies and irrigation channels. A

notable shift of approximately 20 nm in humic-like fluorescence peaks was observed compared to non-black soil regions, reflecting unique molecular structures derived from black soil. Additionally, a significant correlation between total phosphorus (TP) and tyrosine-like peak B ($r \geq 0.85$) suggests the potential for using CDOM spectral features as proxies for nutrient status.

This study is the first to systematically characterize the optical and biochemical features of CDOM in black soil agricultural systems and to clarify its linkage to soil properties and microbial processes. The findings offer practical value for real-time water quality monitoring and provide a scientific foundation for precision agriculture strategies. These include phosphorus fertilizer optimization and the potential development of fluorescence-based tools to assess rhizosphere microbial activity and crop health. Future work should expand spatial sampling and incorporate soil enzymology and microbial ecology to further refine the understanding of CDOM dynamics. Overall, this research contributes valuable insight toward the sustainable management of irrigation, soil fertility, and rice production in black soil regions.

Consent for publication

All authors have agreed with the content and all have given explicit consent to publish.

Data availability

The data that support the findings of this study are available from the corresponding author, upon reasonable request.

Author contributions

Z. L. and C. L. (Chunyu Liu) designed and conducted this study. Z. L. and C. L. (Chunyu Liu) per-formed the data analysis and drafted the manuscript. J. W. and C. L. (Changming Li) provided guidance and revisions to the article. X. T. and Y. T. contributed to the organization of the experi-mental results. All authors have read and agreed to the published version of the manuscript.

Conflicts of interest

There are no conflicts to declare.

Acknowledgements

References

1 N. Ma, *et al.*, Spatial variation in bacterial community and dissolved organic matter composition in groundwater near a eutrophic lake, *Aquat. Ecol.*, 2022, **56**, 555–571.

2 S. K. Ishii and T. H. Boyer, Behavior of reoccurring PARAFAC components in fluorescent dissolved organic matter in natural and engineered systems: a critical review, *Environ. Sci. Technol.*, 2012, **46**, 2006–2017.

3 S. Acharya, *et al.*, Relevance of tributary inflows for driving molecular composition of dissolved organic matter (DOM) in a regulated river system, *Water Res.*, 2023, **237**, 119975.

4 I. F. Creed, *et al.*, Global change-driven effects on dissolved organic matter composition: implications for food webs of northern lakes, *Global Change Biol.*, 2018, **24**, 3692–3714.

5 M. A. Xenopoulos, *et al.*, How humans alter dissolved organic matter composition in freshwater: relevance for the Earth's biogeochemistry, *Biogeochemistry*, 2021, **154**, 323–348.

6 S. R. Brogi, S. Y. Ha, K. Kim, M. Derrien, Y. K. Lee and J. Hur, Optical and molecular characterization of dissolved organic matter (DOM) in the Arctic ice core and the underlying seawater (Cambridge Bay, Canada): Implication for increased autochthonous DOM during ice melting, *Sci. Total Environ.*, 2018, **627**, 802–811.

7 X. Fu, H. Du and H. Xu, Comparison in UV-induced photodegradation properties of dissolved organic matters with different origins, *Chemosphere*, 2021, **280**, 130633.

8 S. A. Lee, J. Lee, Y. Han and G. Kim, Biogeochemical alteration and fluxes of dissolved organic matter and nutrients in coastal bays, *Estuarine, Coastal Shelf Sci.*, 2020, **245**, 106992.

9 A. I. Goranov, M. W. Swinton, D. A. Winkler, J. L. Farrell, S. A. Nierzwicki-Bauer and S. Wagner, Assessing the spatiotemporal variability of dissolved organic matter fluorescence composition in the Lake George, NY watershed, *Biogeochemistry*, 2024, **167**, 849–870.

10 W. Li, X. Li, C. Han, G. Li, H. Wu and M. Li, A new view into three-dimensional excitation–emission matrix fluorescence spectroscopy for dissolved organic matter, *Sci. Total Environ.*, 2023, **855**, 158963.

11 M. Harir, K. M. Cawley, N. Hertkorn, P. Schmitt-Kopplin and R. Jaffé, Molecular and spectroscopic changes of peat-derived organic matter following photo-exposure: effects on heteroatom composition of DOM, *Sci. Total Environ.*, 2022, **838**, 155790.

12 A. R. Pearson, B. R. Fox, M. J. Vandergoes and A. Hartland, The sediment fluorescence–trophic level relationship: using water-extractable organic matter to assess past lake water quality in New Zealand, *N. Z. J. Mar. Freshw. Res.*, 2022, **56**, 213–233.

13 J. Liu, Y. Zhang and H. Zhai, Distribution characteristics and sources of DOM in Bohai Bay seawater during wet season, *China Environ. Sci.*, 2021, **41**, 4802–4810.

14 A. Andersson, *et al.*, Molecular level seasonality of dissolved organic matter in freshwater and its impact on drinking water treatment, *Environ. Sci. Water Res. Technol.*, 2024, **10**, 1964–1981.

15 D. Yuan, *et al.*, Impact of hydrophyte decomposition on the changes and characteristics of dissolved organic matter in lake water, *Ecol. Indic.*, 2020, **116**, 106482.

16 J. Gao, C. Liang, G. Shen, J. Lv and H. Wu, Spectral characteristics of dissolved organic matter in various agricultural soils throughout China, *Chemosphere*, 2017, **176**, 108–116.

17 K. Suman, *et al.*, Characterization of heterogeneity in popular rice landrace through field and molecular evaluation, *Field Crops Res.*, 2023, **304**, 109181.

18 Q. Zhang, W. Qin, W. Cao, J. Jiao, Z. Yin and H. Xu, Response of erosion reduction effect of typical soil and water conservation measures in cropland to rainfall and slope gradient changes and their applicable range in the Chinese Mollisols Region, Northeast China, *Int. Soil Water Conser. Res.*, 2023, **11**, 251–262.

19 J. Zhang, J. Wang, S. Chen, M. Wang, S. Tang and W. Zhao, Integrated risk assessment of agricultural drought disasters in the major grain-producing areas of Jilin Province, China, *Land*, 2023, **12**, 160.

20 X. Li, Z. Shi, Z. Xing and M. Wang, Dynamic evaluation of cropland degradation risk by combining multi-temporal remote sensing and geographical data in the Black Soil Region of Jilin Province, China, *Appl. Geogr.*, 2023, **154**, 102920.

21 C. Li, *et al.*, Fertilization restructures nematode assemblages by modifying soil pH in croplands of Northeast China, *Front. Environ. Sci.*, 2023, **11**, 2023.

22 Y. P. Chin, G. Aiken and E. O'Loughlin, Molecular weight, polydispersity, and spectroscopic properties of aquatic humic substances, *Environ. Sci. Technol.*, 1994, **28**, 1853–1858.

23 J. R. Helms, A. Stubbins, J. D. Ritchie, E. C. Minor, D. J. Kieber and K. Mopper, Absorption spectral slopes and slope ratios as indicators of molecular weight, source, and photobleaching of chromophoric dissolved organic matter, *Limnol. Oceanogr.*, 2008, **53**, 955–969.

24 Y. Chen, N. Senesi and M. Schnitzer, Information provided on humic substances by E_4/E_6 ratios, *Soil Sci. Soc. Am. J.*, 1977, **41**, 352–358.

25 E. E. Lavonen, D. N. Kothawala, L. J. Tranvik, M. Gonsior, P. Schmitt-Kopplin and S. J. Köhler, Tracking changes in the optical properties and molecular composition of dissolved organic matter during drinking water production, *Water Res.*, 2015, **85**, 286–294.

26 R. M. Cory and D. M. McKnight, Fluorescence spectroscopy reveals ubiquitous presence of oxidized and reduced quinones in dissolved organic matter, *Environ. Sci. Technol.*, 2005, **39**, 8142–8149.

27 A. Huguet, L. Vacher, S. Relexans, S. Saubusse, J. M. Froidefond and E. Parlanti, Properties of fluorescent dissolved organic matter in the Gironde Estuary, *Org. Geochem.*, 2009, **40**, 706–719.

28 J. E. Birdwell and K. T. Valsaraj, Characterization of dissolved organic matter in fogwater by excitation–emission matrix fluorescence spectroscopy, *Atmos. Environ.*, 2010, **44**, 3246–3253.

29 T. Ohno, I. J. Fernandez, S. Hiradate and J. F. Sherman, Effects of soil acidification and forest type on water soluble soil organic matter properties, *Geoderma*, 2007, **140**, 176–187.

30 L. Serène, *et al.*, Transit Time index (TTi) as an adaptation of the humification index to illustrate transit time differences in karst hydrosystems: application to the karst springs of the Fontaine de Vaucluse system (southeastern France), *Hydrol. Earth Syst. Sci.*, 2022, **26**, 5035–5049.

31 HJ 670-2013, *National Environmental Protection Standards of the People's Republic of China, Water Quality-Determination of Orthophosphate and Total Phosphorus-Continuous Flow analysis(CFA) and Ammonium Molybdate Spectrophotometry*, Ministry of Ecology and Environment of the People's Republic of China, Beijing, China, 2015.

32 HJ 636-2012, *National Environmental Protection Standards of the People's Republic of China, Water Quality-Determination of Total Nitrogen-Alkaline Potassium Persulfate Digestion UV Spectrophotometric Method*, Ministry of Ecology and Environment of the People's Republic of China, Beijing, China, 2012.

33 HJ 535-2009, *National Environmental Protection Standards of the People's Republic of China, Water quality–Determination of Ammonia nitrogen–Nessler's Reagent Spectrophotometry*, Ministry of Ecology and Environment of the People's Republic of China, Beijing, China, 2009.

34 HJ 501-2009, *National Environmental Protection Standards of the People's Republic of China, Water Quality—Determination of Total Organic Carbon—Combustion Oxidation Nondispersive Infrared Absorption Method*, Ministry of Ecology and Environment of the People's Republic of China, Beijing, China, 2009.

35 HJ 636-2012, *National Standard of the People's Republic of China, Standard for Ground Water Quality*, State Administration for Market Regulation of the People's Republic of China & Standardization Administration of the People's Republic of China, Beijing, China, 2017.

36 M. Kida, *et al.*, Origin, distributions, and environmental significance of ubiquitous humic-like fluorophores in Antarctic lakes and streams, *Water Res.*, 2019, **163**, 114901.

37 D. Omanović, S. Marcinek and C. Santinelli, TreatEEM—A software tool for the interpretation of fluorescence excitation–emission matrices (EEMs) of dissolved organic matter in natural waters, *Water*, 2008, **15**, 2214.

38 K. R. Murphy, C. A. Stedmon, T. D. Waite and G. M. Ruiz, Distinguishing between terrestrial and autochthonous organic matter sources in marine environments using fluorescence spectroscopy, *Mar. Chem.*, 2023, **108**, 40–58.

39 A. Baker and M. Curry, Fluorescence of leachates from three contrasting landfills, *Water Res.*, 2004, **38**, 2605–2613.

40 A. Baker, Fluorescence excitation– emission matrix characterization of some sewage-impacted rivers, *Environ. Sci. Technol.*, 2001, **35**, 948–953.

41 H. Jiang, T. Zhang and F. Yang, Characteristics of fluorescence and ultraviolet spectra during domestic wastewater treatment process, *Environ. Sci. Technol.*, 2019, **42**, 151–156.

42 C. Nima, *et al.*, CDOM absorption properties of natural water bodies along extreme environmental gradients, *Water*, 2019, **11**, 1988.

43 N. Patel-Sorrentino, S. Mounier and J. Y. Benaim, Excitation–emission fluorescence matrix to study pH influence on organic matter fluorescence in the Amazon basin rivers, *Water Res.*, 2002, **36**, 2571–2581.

44 S. A. Timko, M. Gonsior and W. J. Cooper, Influence of pH on fluorescent dissolved organic matter photo-degradation, *Water Res.*, 2015, **85**, 266–274.

45 R. V. Khose, G. Chakraborty, M. P. Bondarde, *et al.*, Red-fluorescent graphene quantum dots from guava leaf as a turn-off probe for sensing aqueous, *New J. Chem.*, 2021, **45**, 4617–4625.